Thermochimica Acta 484 (2009) 48–56

Contents lists available at ScienceDirect

Thermochimica Acta

journal homepage: www.elsevier.com/locate/tca

Crystallization behavior of polyamide 6/halloysite nanotubes nanocomposites

Baochun Guo*, Quanliang Zou, Yanda Lei, Mingliang Du, Mingxian Liu, Demin Jia

Department of Polymer Materials and Engineering, South China University of Technology, Guangzhou 510640, China

ARTICLE INFO

Article history:
Received 22 August 2008
Received in revised form
19 November 2008
Accepted 3 December 2008
Available online 11 December 2008

Keywords:
Polyamide 6
Halloysite
Nanocomposite
Crystallization
Effective activation energy
Polymorphism

ABSTRACT

Non-isothermal crystallization and the polymorphism of the PA6 and the polyamide 6/halloysite nanotubes (PA6/HNTs) nanocomposites are studied by adopting differential scanning calorimetry (DSC) analysis, X-ray diffraction (XRD) analysis and polarized optical microscopy (POM) observations. HNTs act as nucleating agent and accelerate the crystallization. The kinetics analysis indicates that the fold-surface free energy of PA6/HNTs nanocomposites is larger than that of neat PA6. The increasing tendency of the fold-surface free energy of PA6/HNTs nanocomposites is restricted at higher HNTs loading. Interestingly, the crystallinity of the PA6/HNTs nanocomposites increases with cooling rate. HNTs content is found to have a significant effect upon the crystallinity of the PA6/HNTs nanocomposites, and the crystallinity reaches its maximum with 5 phr of HNTs content. Moreover, the higher HNTs content is, the larger percentage γ-phase crystals take up. The crystallization behavior of the PA6/HNTs nanocomposites is correlated with the multiple roles of HNTs in the crystallization of PA6.

1. Introduction

Polyamide 6 (PA6) with high fatigue strength, low coefficient of friction and high resistance to a wide spectrum of fuels, oils, and chemicals, is an important semicrystalline engineering plastics and finds its applications in auto parts, parts for electrical appliances, construction materials, transportation materials and fiber materials and the like. It is well known that PA6 has an interesting polymorphism behavior. As early as in 1947, Bunn and Garner [1] found that PA6 had α-phase and γ-phase crystals. The α-phase crystals constituted the more thermodynamically stable phase, and adopted a fully extended configuration with anti-parallel chains linked by hydrogen bonds to adjacent chains. The γ-phase crystal of PA6 [2], which was less stable (metastable) than α-phase and could be converted to the α-phase by annealing, was formed by hydrogen bonds between parallel adjacent chains.

In recent years, PA6 nanocomposites have drawn much attention due to their unprecedented performance compared with their microcomposite counterparts. The PA6 nanocomposites with inclusions of carbon nanotubes (CNTs) [3–7] and organic montmorillonite (O-MMT) [8–11] have been intensively investigated. Previously we reported PA6 nanocomposites incorporating of halloysite nanotubes (HNTs) with excellent physical and mechanical properties prepared by traditional melt blending [12]. It is well known that the physical and mechanical properties of semicrystalline polymer are, to a large degree, defined by its morphology, crystalline structure and crystallinity. Nanosized inclusions, such as CNTs and O-MMT, show profound effects on the crystallization behavior of PA6. For example, CNTs in PA6/CNTs nanocomposites [3,13] function as heterogeneous nucleating agent and accelerate the formation of α-phase crystals, with the absence of γ-phase crystals. Besides, numerous studies on crystallization kinetics of PA6 with nanosized inclusions have been conducted [14–22]. For instance, Fang ZP et al. [16,17] have studied the isothermal and non-isothermal crystallization behaviors of PA6/CNT nanocomposites. Their results indicate that under the non-isothermal crystallization conditions CNTs act as nucleating agent, leading to higher initial crystallization temperature (T_0) and prolonged half crystallization time ($t_{1/2}$). It can thus be inferred that CNT nanotubes hinder the mobility of PA chains and consequently slow down the crystallization. By contrast, under the isothermal crystallization conditions, $t_{1/2}$ is shortened. As for PA6/O-MMT nanocomposites [18–20], montmorillonite serves as nucleation and facilitates the formation γ-phase crystals. Paul et al. [21] and Wu et al. [22] have conducted detailed studies on the non-isothermal crystallization kinetics of PA6/O-MMT nanocomposites. The PA6/O-MMT nanocomposites show complicated crystallization mechanism. Significantly shortened $t_{1/2}$ and minimally changed T_0 are observed for the nanocomposites.

HNTs, a type of tubular nanoclay, have been recognized as the additive of polymers for better mechanical properties or thermal properties [23–26]. The present work attempts to study the crystallization behaviors including non-isothermal crystallization kinetics and polymorphism of PA6/HNTs nanocomposites. Such empirical

* Corresponding author. Fax: +86 20 2223 6688.
E-mail address: psbcguo@scut.edu.cn (B. Guo).

0040-6031/$ – see front matter © 2008 Elsevier B.V. All rights reserved.
doi:10.1016/j.tca.2008.12.003

kinetics equations as Avrami equation and Mo equation are used for the analysis of the dependences of crystallization rate and temperature of the nanocomposites on the HNTs content and cooling rate. In addition, wide angle X-ray diffraction (WXRD) is employed to disclose the dependences of the crystallinity and the polymorphism of the nanocomposites on the cooling rate and the HNTs loading during the non-isothermal crystallization process. The crystallization behavior of the nanocomposites is correlated to the interactions between HNTs and PA6 chains.

2. Experimental

2.1. Materials

HNTs, mined in Yichang, Hubei Province of China, were finely ground and dried for 12 h at 80 °C. PA6 (ZISAMIDE TP6603), with molecular weight of 22700, was purchased from JI SHENG Co., Ltd., Taiwan and dried for 12 h at 80 °C before blending with HNTs.

2.2. Preparation of PA6/HNTs nanocomposites

The blends of PA6 and HNTs with designed composition were extruded with a twin-screw extruder and pelletized. The extrusion temperatures were set at 200 °C, 240 °C, 240 °C, 240 °C, 235 °C, 235 °C, 230 °C and 230 °C from hopper to die, respectively. The code of PA6/HNTsX represented the PA6/HNTs nanocomposite with X parts HNTs relative to 100 parts of PA6.

2.3. Differential scanning calorimetry (DSC) procedures

The non-isothermal crystallization of PA6/HNTs composites was analyzed by means of DSC TAQ 20. Before testing, all the samples were dried at 80 °C for 12 h to remove moisture. All DSC analyses were performed under nitrogen purging. The non-isothermal crystallization of PA6/HNTs nanocomposites was conducted as follows. The samples were heated from ambient temperature to 250 °C at a heating rate of 40 °C/min. The samples were kept for 5 min at this temperature to eliminate the thermal history. Then the samples were cooled to ambient temperature at a constant cooling rate of 2.5 °C/min, 5 °C/min, 10 °C/min, 20 °C/min, and 40 °C/min. The thermograms were recorded for the calculation of the non-isothermal crystallization kinetics.

In order to determine the equilibrium melting temperature (T_m^0), the isothermal crystallization of PA6/HNTs nanocomposites and subsequent melting behaviors were performed as follows. The sample was heated to 250 °C at a rate of 40 °C/min and held at this temperature for 5 min to eliminate any thermal history, and then jump to the predetermined cryatallization temperature (T_c), ranged from 200 °C to 192 °C in steps of 2 °C and was maintained at T_c for 30 min necessary for the DSC trace to return to the calorimeter baseline. The specimens were subsequently cooled to 30 °C at a rate of 40 °C/min and then heated to 250 °C at a rate of 10 °C/min.

2.4. X-ray diffraction

The X-ray diffraction (XRD) patterns were recorded using the PANalytical X'pert PRO X-RAY Diffractometer. The Cu Kα radiation source was operated at 40 kV and a current of 40 mA. Patterns were recorded by monitoring those diffractions that appeared from 5° to 30°. The scan speed was 1°/min. The samples for XRD were prepared in the DSC chamber and the settings are the same as those in the non-isothermal crystallization in DSC experiments. Data of XRD were analyzed by use of origin 7.0 Peak Fitting Module, the values of 2θ of α-phase crystals were estimated as 19.9° ± 0.1 (α1) and 23.6° ± 0.1(α2) and the values of 2θ of γ-phase crystals and amorphous diffraction peak as 21.3° ± 0.1 and 21.5° ± 0.2, respectively.

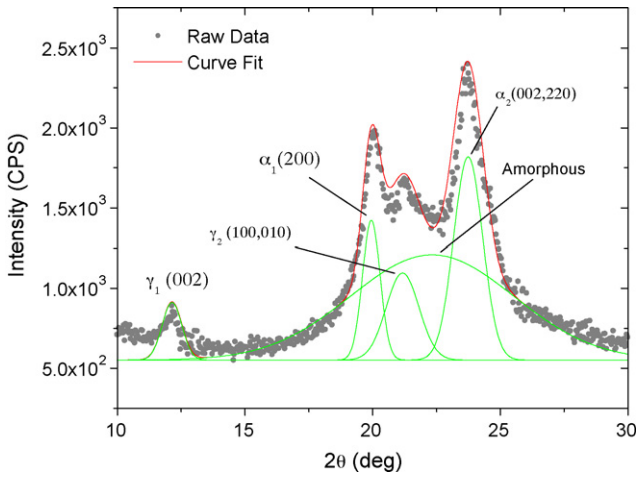

Fig. 1. XRD pattern and the profile fitting technique used to deconvolute the amorphous and crystalline phases (PA6/HNTs10 specimen at the cooling rate of 2.5 °C/min).

Each peak was modeled by using a Gaussian peak shape. The area of each peak was calculated, the crystallinity, and the proportions of each crystal form could be estimated [27,28]. The deconvolution of the XRD curve is shown in Fig. 1.

2.5. Polarized optical microscopy (POM)

The crystalline morphologies of neat PA6 and PA6/HNTs nanocomposites were observed by using a polarized optical microscope (Olympus BX51 system). The samples were melted at 250 °C between two glass slides to obtain thin films with the thickness about 50 μm and maintained at this temperature for 10 min, after that the samples were cooled to 205 °C at a constant cooling rate of 40 °C/min, and maintained at this temperature for 30 min, then cooled to ambient temperature at a constant cooling rate of 40 °C/min.

2.6. Theoretical background for non-isothermal crystallization kinetics

2.6.1. Avrami model and the modified models

Many models have been proposed to study the non-isothermal crystallization of polymer. The most common approach is Avrami equation [29]. It is expressed as follows:

$$\log[-\ln(1 - X_t)] = \log Z_t + n \log t \quad (1)$$

where X_t stands for crystallinity at time of t, n for index of Avrami which is determined by nucleation and growth process parameters, t for time and Z_t for rate constant. However, since Avrami equation is based upon isothermal crystallization mode, considering the characterizations of non-isothermal process, Jeziorny [30] introduce the cooling rate φ to correct the crystallization rate constant:

$$\log Z_c = \frac{\log Z_t}{\varphi} \quad (2)$$

Thus, Avrami equation can be used to analyze the non-isothermal system.

Furthermore, Ozawa [31,32] with the assumption of a constant cooling rate transforms the equation by taking into consideration the impact of cooling rate to make it applicable for the non-isothermal crystallization. Ozawa equation is expressed as:

$$\log[-\ln(1 - X_t)] = \log K(T) - m \log \varphi \quad (3)$$

where X_t stands for crystallinity at time of t, m for index of Ozawa similar to Avrami exponent, φ for cooling rate and $K(T)$ for the func-

tion of cooling rate. $\log[-\ln(1-X_t)]$ as a function of $\log\varphi$ makes it possible to obtain the values of the index m and the kinetic parameter $K(T)$. However, if cooling rate changes in a wide range, $\log[-\ln(1-X_t)]$ versus $\log\varphi$ cannot display a linear relation, and the index m and the kinetic parameter $K(T)$ cannot be calculated.

Since Avrami equation relates X_t to t and Ozawa equation relates X_t to φ, Mo and his colleagues [33] believe that the two equations can be combined into one according to the relationship between t and φ. Here goes Mo equation:

$$\log\ \varphi = \log F(T) - \delta \log t \tag{4}$$

Here:

$$F(T) = \left[\frac{K(T)}{Z_t}\right]^{1/m}, \qquad \delta = n/m \tag{5}$$

In this equation, the velocity parameter $F(T)$ refers to the needed cooling rate to reach a defined crystallinity at unit crystallization time. On the basis of Mo equation, with a given crystallinity, $\log\varphi$ as a function of $\log t$ displays linear function, in which $\log F(T)$ represents the intercept of the line and $-\delta$ its gradient.

2.7. Evaluation of Hoffman–Lauritzen parameters of non-isothermal crystallization

Avrami related models can only evaluate the overall rate and activation energy of the non-isothermal crystallization. The single value of the activation energy could not adequately represent the crystallization process. Such problem could be eliminated by isoconversional method, through which the physically meaningful parameters for the crystallization could be evaluated.

Based on the Hoffman–Lauritzen theory [34], that the linear growth rate of a polymer crystal, G depends on temperature, T as follows:

$$G = G_0\ \exp\left(\frac{-U^*}{R(T-T_\infty)}\right)\ \exp\left(\frac{-K_g}{T\,\Delta T f}\right) \tag{6}$$

Where G_0 is the pre-exponential factor, U^* is the activation energy of the segmental jump, $\Delta T = T_m^0 - T$ is the under-cooling, $f = 2T/(T_m^0 - T)$ is the correction factor, T_∞ is a hypothetical temperature at which viscous flow ceases (usually [34] taken 30 K below the glass transition temperature, T_g). The kinetic parameter K_g has the following form:

$$K_g = \frac{nb\sigma\sigma_e T_m^0}{\Delta h_f^0\ k_B} \tag{7}$$

where n takes the value 4 for crystallization regime I and III, and 2 for regime II; b is the distance between two adjacent fold planes; σ and σ_e are the lateral and folding surface free energy, T_m^0 is the equilibrium melting temperature, Δh_f^0 is the heat of fusion per unit volume of crystal, k_B is the Boltzmann constant. The parameters U^* and K_g are usually determined by measuring microscopically the growth rate in a series of non-isothermal runs and substituting the measured value in rearranged Eq. (6):

$$\ln\ G + \frac{U^*}{R(T-T_\infty)} = \ln G_0 - \frac{K_g}{T\,\Delta T f} \tag{8}$$

And in narrow temperature region, an explicit dependence of effective activation energy (E) on T can be derived from Eq. (6) as follows [35]:

$$E_\alpha(T) = -R\frac{\mathrm{d}\ln G}{\mathrm{d}T^{-1}} = U^*\frac{T^2}{(T-T_\infty)^2} + K_g R\frac{(T_m^0)^2 - T^2 - T_m^0 T}{\Delta T^2\ T} \tag{9}$$

where E_α represents the effective activation energy when the crystallinity degree is α.

Based on non-linear isoconversional method [36], the effective activation energy for the non-isothermal crystallization is calculated in accordance with Eq. (10) and the specific derivation process can be figured out by using as Refs. [37,38]:

$$\Omega(E_\alpha) = \min\left|\sum_{i=1}^{n}\sum_{j\neq i}^{n}\frac{\varphi_j \bullet I(E_\alpha, T_{\alpha,i})}{\varphi_i \bullet I(E_\alpha, T_{\alpha,j})} - n(n-1)\right| \tag{10}$$

Here

$$I(E_\alpha, T_\alpha) = \int_{T_0}^{T_\alpha} \exp\left(\frac{-E_\alpha}{RT_\alpha}\right)\ \mathrm{d}T$$

This integral is determined with the help of a Doyle's approximation [39].

$$I(E_\alpha, T_\alpha) \cong \frac{E_\alpha}{R}\exp\left(-5.331 - 1.052\frac{E_\alpha}{RT_\alpha}\right) \tag{11}$$

And φ stands for the cooling rate; n represents the number of cooling rates, in the present study is 5. By substituting a series of different φ_i, $T_{\alpha,i}$ (i = 1, 2, . . ., n) estimated at the same α on the DSC curves into Eq. (10), we can obtain the minimum value of E_α.

3. Results and discussion

3.1. Non-isothermal crystallization kinetics

Fig. 2 presents DSC thermograms of neat PA6 and PA6/HNTs5 nanocomposites, from which values of the initial crystallization temperature (T_0), the peak temperature (T_p), crystallization temperature range (D), and the crystallization enthalpy (ΔH) are all received and summarized in Table 1. From Table 1, it can be seen that T_0 and T_p of PA6 and its nanocomposites are decreased with the increasing cooling rate. Besides, at the same cooling rate, T_0 and T_p of PA6/HNTs nanocomposites are higher than those of neat PA6, indicating nucleating effect of HNTs. In addition, the range of the crystallization exotherms D of the nanocomposites is smaller than that of the neat PA6, suggesting faster overall crystallization. Moreover, when the content of HNTs is 5 phr, T_0 and T_p reach the peak values, and following that, the higher the HNTs content is, the lower T_0 and T_p become. However, T_0 and T_p are still higher than those of

Table 1
Values of ΔH, T_0, T_p, and D at various cooling rates for neat PA6 and its nanocomposites.

Sample	φ (°C/min)	ΔH (J/g)	T_0 (°C)	T_p (°C)	D (°C)
Neat PA6	2.5	67.83	200.67	195.56	14.79
	5	64.98	197.41	191.26	18.05
	10	61.56	194.67	186.59	25.11
	20	60.99	190.14	181.00	35.89
	40	59.47	184.88	174.32	47.45
PA6/HNTs2	2.5	49.08	201.95	198.39	10.32
	5	52.48	198.12	194.28	12.24
	10	54.80	194.40	189.85	17.05
	20	57.67	190.89	184.86	28.35
	40	58.99	185.38	178.54	42.42
PA6/HNTs5	2.5	53.74	202.20	198.60	10.31
	5	55.37	199.44	194.83	13.31
	10	55.55	196.18	190.82	19.08
	20	57.36	192.65	186.13	26.85
	40	59.71	187.89	180.46	42.17
PA6/HNTs10	2.5	49.92	201.20	197.71	9.55
	5	51.30	198.19	193.74	13.07
	10	52.85	195.43	189.44	22.11
	20	53.37	191.15	184.42	27.86
	40	56.31	185.88	178.35	42.16

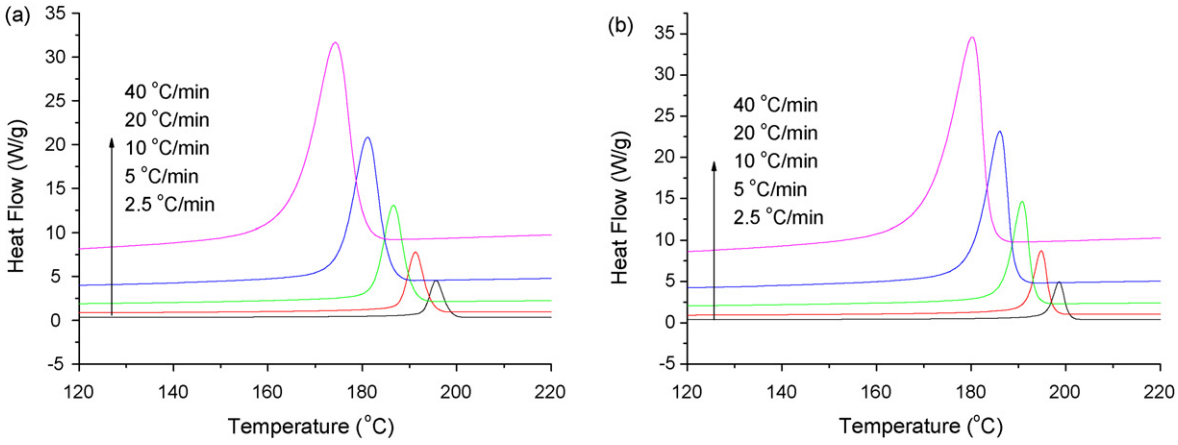

Fig. 2. DSC thermograms of non-isothermal crystallization at different cooling rates for (a) neat PA6 and (b) PA6/HNTs5.

neat PA6. The above characteristics may be attributed to the dual roles of HNTs in determining the crystallization process. On one hand, HNTs work as nucleating agent, and on the other hand, the strong hydrogen bonding interaction between HNTs and PA6 chains restricts the mobility of PA6 chains. When there is a small amount of HNTs content, nucleating effect of HNTs dominates, resulting in higher T_0 and T_p. When HNTs content is sufficiently high, the restricting effect of HNTs dominates, leading to lower T_0 and T_p.

Fig. 3 presents the $(1 - X_t)$ as a function of time for neat PA6 and PA6/HNTs5 nanocomposites crystallized at various cooling rates. It is revealed the cooling rate plays an important role in the crystallization process, which is in accordance with the results of PA6/MMT systems [22,40]. In addition, the platform in the later periods is caused by the impingement among spherulites when the crystal grains grow. What is more, half crystallization time ($t_{1/2}$) from Fig. 3 is summarized in Table 2. As shown in Table 2, for both neat PA6 and PA6/HNTs nanocomposites, the higher cooling rate is, the smaller $t_{1/2}$ (or crystallization time range) becomes. In addition, it is obvious that at the same cooling rate the $t_{1/2}$ of PA6/HNTs nanocomposites is shorter than that of neat PA6. It is noticeable that PA6/HNTs5 has longer $t_{1/2}$ than other PA6/HNTs nanocomposites. The variation of $t_{1/2}$ may be explained as follows. The crystallization process consists of nucleation and crystal growth. The surface of HNTs is covered with –Si–O and –OH groups which have a strong interaction with amide group in PA6 chains via hydrogen bonding. As a consequence, PA6 chains may display an orderly arrangement on the surface of HNTs, resulting accelerated nucleation and hindered crystal growth. Therefore, when the content of HNTs is lower, crystallization process is mainly controlled by crystal growth since there are not so many nuclei. When the content of HNTs is higher, crystallization process is mainly controlled by nucleation due to the large amount of nuclei that leave crystal little space to growing. PA6/HNTs5 nanocomposite, which may possess balanced nucleation and crystal growth, show longest $t_{1/2}$ among all the nanocomposites. The same accelerating effect holds true to PA6/O-MMT nanocomposites [22] but contradictory to PA6/CNTs nanocomposites [16]. The reason is probably that montmorillonite has similar surface chemistry with HNTs and has strong interaction with PA6 chains. As a comparison, CNTs, having no strong interaction with PA6 chains, can greatly improve PA6 initial crystallization temperature (t_0) and can somewhat hinder the movement of PA6 molecules as well, thus making the $t_{1/2}$ longer than that of neat PA6.

Table 2
Values of n, Z_c, and $t_{1/2}$ at various cooling rates for neat PA6 and its nanocomposites.

φ (°C/min)	n	Z_c	$t_{1/2}$ (min)	φ (°C/min)	n	Z_c	$t_{1/2}$ (min)
Neat PA6				PA6/HNTs5			
2.5	3.7	0.28	2.13	2.5	4.0	0.29	1.89
5	3.7	0.75	1.31	5	3.9	0.82	1.12
10	3.8	1.03	0.81	10	4.2	1.13	0.67
20	3.7	1.11	0.5	20	4.3	1.19	0.4
40	3.8	1.09	0.33	40	3.9	1.13	0.26
PA6/HNTs2				PA6/HNTs10			
2.5	4.2	0.29	1.83	2.5	3.8	0.35	1.72
5	4.0	0.87	1.05	5	3.7	0.87	1.04
10	4.1	1.15	0.63	10	4.1	1.14	0.64
20	3.7	1.17	0.37	20	3.9	1.17	0.39
40	3.6	1.12	0.25	40	3.7	1.12	0.26

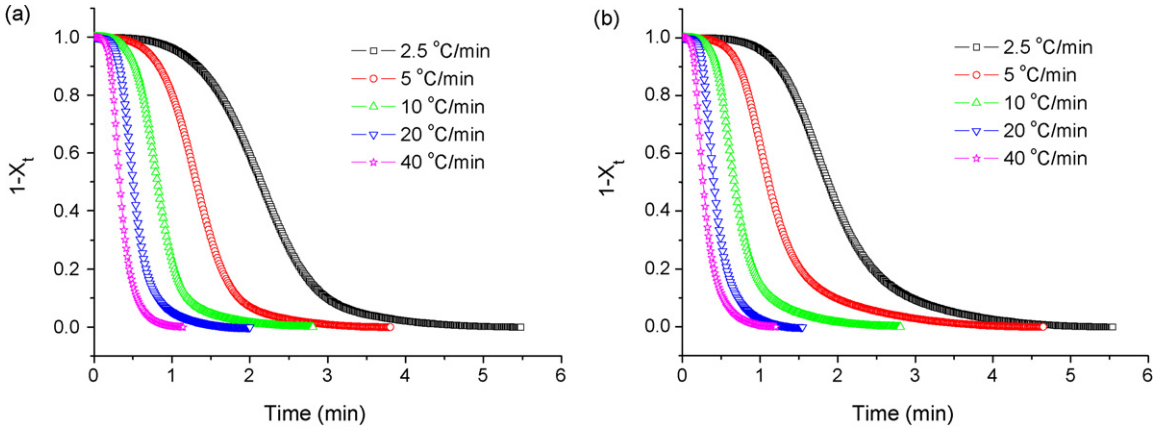

Fig. 3. Plots of $(1 - X_t)$ as a function of time for (a) neat PA6 and (b) PA6/HNTs5.

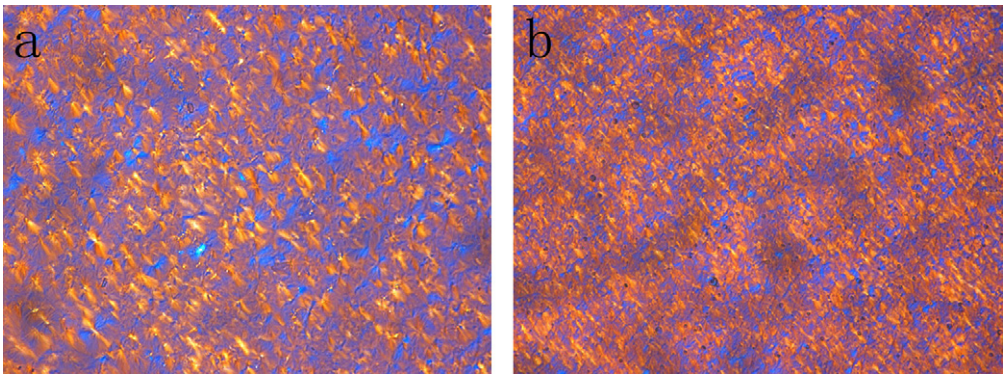

Fig. 4. POM micrographs of (a) neat PA6 and (b) PA6/HNTs5.

The nucleation effect of HNTs may be substantiated by the POM observations. As shown in Fig. 4, classical Maltese cross patterns are observed in neat PA6 and PA6/HNTs nanocomposites by POM. Obviously, the well-developed spherulites can be observed in neat PA6 and the diameter fairly larger than that in the nanocomposite, suggesting much more nucleus in PA6/HNTs nanocomposite.

Fig. 5 shows the plots of $\log[-\ln(1-X_t)]$ as a function of $\log t$ for neat PA6 and PA6/HNTs nanocomposites under the non-isothermal crystallization conditions. Although they are not linear relationship in all range, the coefficient of determinations of linear fit in the crystallinity range of 10–80% is large than 0.996. In view of that, values of Avrami index n and the corresponding velocity parameter Z_c can be calculated in this range, and the results are listed in Table 2. It can be seen that n value ranges of neat PA6 and the nanocomposites are 3.7–3.8 and 3.6–4.3, respectively, indicating more complicated mechanisms of nucleation and crystal growth in the nanocomposites. The higher Z_c is, the higher the crystallization rate becomes. At the same cooling rate Z_c of PA6/HNT nanocomposites is higher than that of neat PA6. Therefore, it is concluded that HNTs accelerate the crystallization of PA6 under the non-isothermal crystallization conditions.

Fig. 6 shows the plots of $\log\varphi$ as a function of $\log t$. Whether for neat PA6 or for PA6/HNTs nanocomposites, $\log\varphi$ and $\log t$ display a linear relation. The values of velocity parameter $F(T)$ and

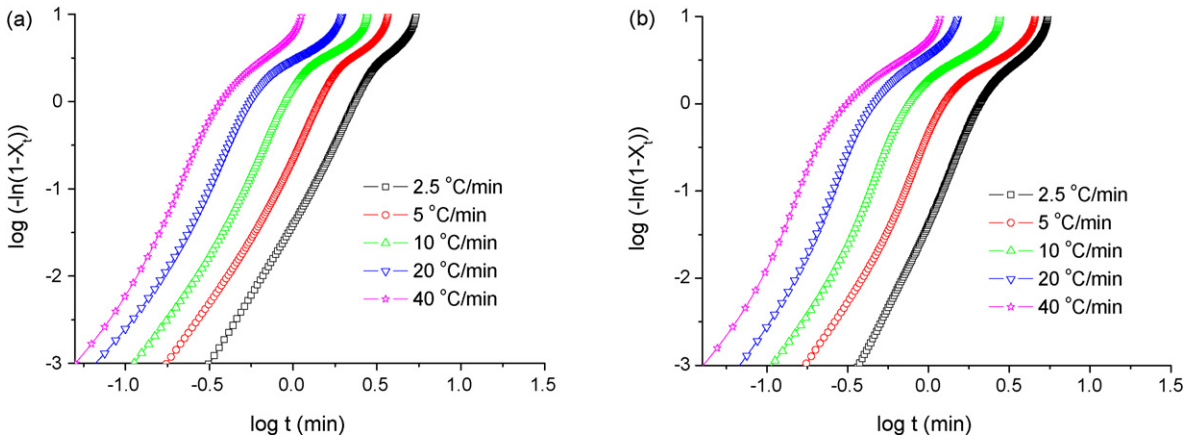

Fig. 5. Plots of $\log[-\ln(1-X_t)]$ as a function of $\log t$ for (a) neat PA6 and (b) PA6/HNTs5.

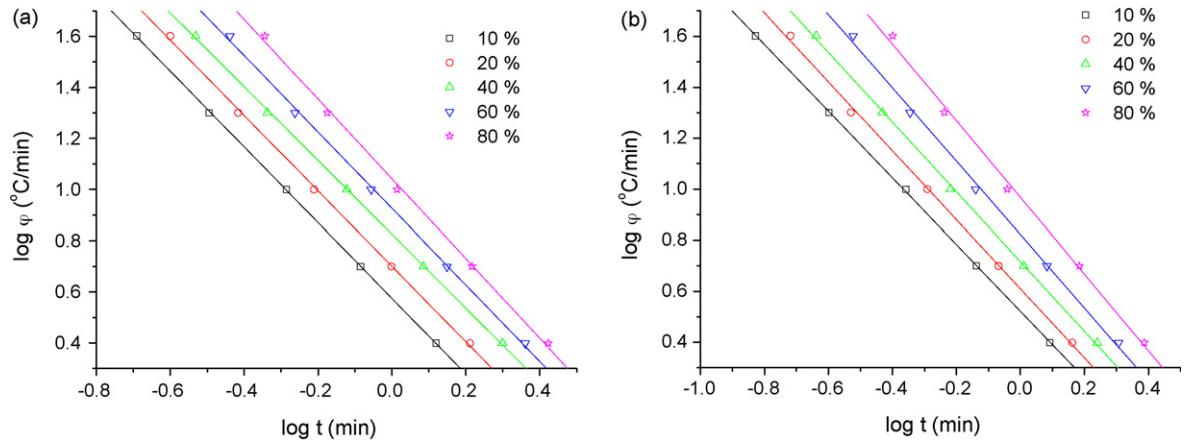

Fig. 6. Plots of $\log\varphi$ as a function of $\log t$ for (a) neat PA6 and (b) PA6/HNTs5.

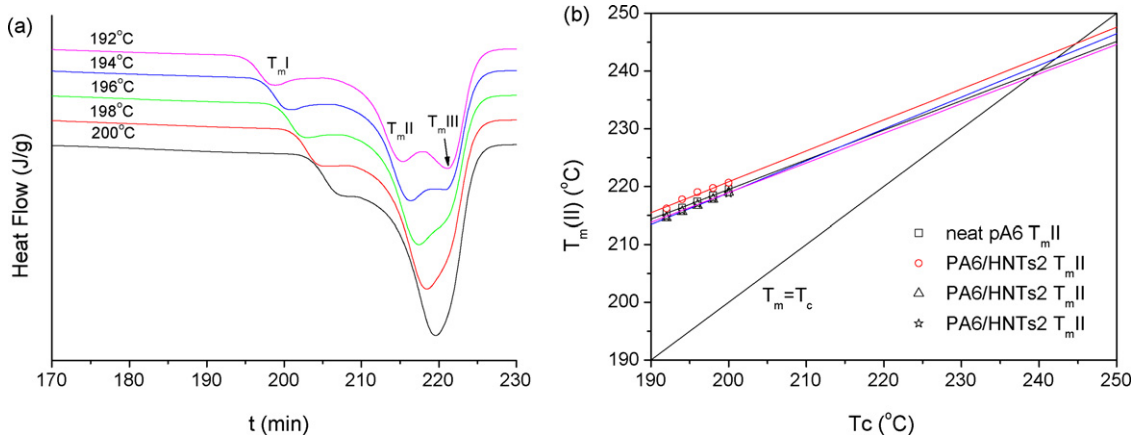

Fig. 7. (a) DSC heating thermograms of neat PA6 and (b) melting temperature as a function of crystallization temperature for neat PA6 and its nanocomposites.

Table 3
Values of $F(T)$ and δ from Mo equation for neat PA6 and PA6/HNTs nanocomposites.

X_t (%)	Neat PA6		PA6/HNTs2		PA6/HNTs5		PA6/HNTs10	
	δ	$F(T)$	δ	$F(T)$	δ	$F(T)$	δ	$F(T)$
10	1.48	3.75	1.24	3.19	1.31	3.32	1.38	2.94
20	1.48	5.01	1.26	3.80	1.35	4.07	1.37	3.71
40	1.45	6.68	1.31	4.85	1.37	5.20	1.42	4.81
60	1.50	8.43	1.42	6.20	1.44	6.64	1.49	6.13
80	1.56	11.02	1.49	8.84	1.50	9.29	1.57	8.61

Table 4
Kinetic data for non-isothermal crystallization of neat PA6 and its nanocomposites.

Sample	Neat PA6	PA6/HNTs2	PA6/HNTs5	PA6/HNTs10
U^* (J/mol)	6222.65	11689.3	10971.61	10466.42
K_g ($10 \times 5\,K^2$)	2.33	3.07	2.74	2.4
R^2	0.99483	0.99867	0.99892	0.99855
T_m^0 (K)	513	517.83	515.22	511.9
$\sigma\sigma_e$ (10^{-4} J^2/m^4)	2.12	2.77	2.50	2.19
σ_e (10^{-3} J/m^2)	6.4	8.4	7.6	6.6

δ are listed in Table 3. It can be found that, the higher the given degree of crystallinity is, the higher the value of $F(T)$ becomes. In other words, higher cooling rate is required so as to get higher crystallinity at the unit crystallization time. In addition, the value of δ is comparatively constant. In contrast with neat PA6, with the same crystallinity, the value of $F(T)$ for PA6/HNTs nanocomposites is still lower. Similarly, it can be inferred that the crystallization rate of PA6/HNTs nanocomposites is higher than that of neat PA6 under the non-isothermal crystallization conditions. This phenomenon will be further explained in the XRD analysis.

3.2. Evaluation of the Hoffman–Lauritzen parameters of non-isothermal crystallization

In order to apply the Hoffman–Lauritzen theory, the equilibrium melting temperature (T_m^0) is firstly evaluated by the isothermal crystallization. According to Hoffman–Weeks, T_m^0 can be obtained by linear extrapolation of T_m versus T_c data to intersect the line $T_m = T_c$ and the intersection point is the T_m^0. Fig. 7(a) presents DSC heating scans of neat PA6. It can be clearly seen that DSC heating curves of PA6 exhibited three melting peaks and that as T_mII is the main melting peak, the value of T_m^0 is determined by extrapolation of the melting temperature (T_mII) versus crystallization temperature. As exhibited in Fig. 7(b), the T_m^0 of neat PA6 and its nanocomposites are available and summarized in Table 4.

Fig. 8(a) displays the E_α dependence obtained from DSC data on non-isothermal crystallization of neat PA6 and its nanocomposite. Depending on the cooling rate, the same value of α is accomplished at different temperatures, which have been used to evaluate an average temperature associated with the α value. The resulting T versus α dependence is shown in Fig. 8(a) too. This dependence allows us to correlate the obtained E_α values with temperature as required by Eq. (9).

Fig. 8(a) exhibits that the absolute value of E_α of neat PA6 and its nanocomposites decreases as crystallinity increases and at the same crystallinity the absolute value of E_α of PA6/HNTs nanocomposites

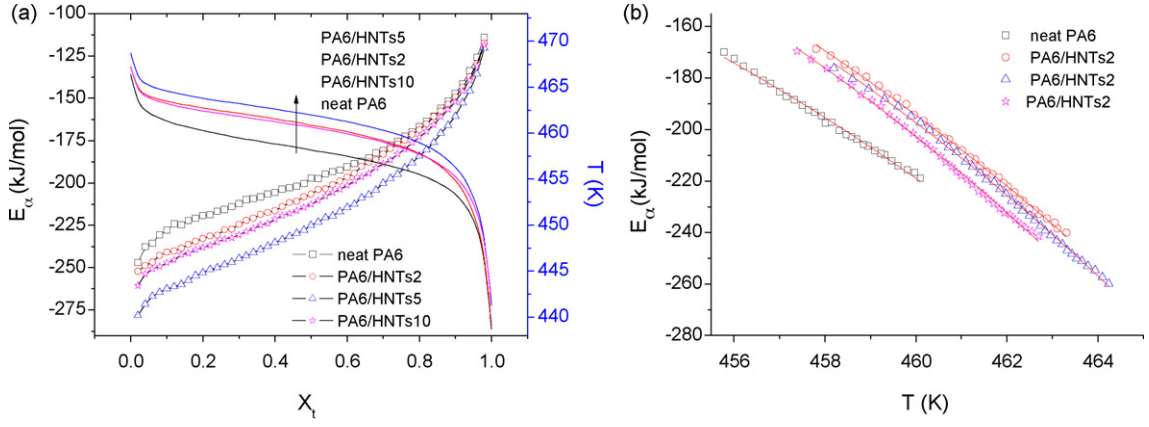

Fig. 8. (a) Dependence of the effective activation energy on the relative extent of crystallization. The solid line represents the variation of the average temperature with the relative extent of crystallization and (b) dependence of the effective activation energy on average temperature. The solid lines represent fits of Eq. (9).

are always higher than that of neat PA6. Besides, the absolute value of E_α of PA6/HNTs nanocomposites tends to decrease as the loading HNTs increase. It indicates that there is a somewhat strong interaction between HNTs and PA6 molecule segments confining the free movement of the latter. However, the interaction intensity tends to decrease at higher HNTs loading.

After the relation of E_a and T is obtained from Fig. 8(a), the values of U^* and K_g can be obtained as well by fitting the Eq. (9) with Origin7.5 software as shown in Fig. 8(b) and the results are summarized in Table 4. Since the crystallizing regime of neat PA6 cannot be determined from Fig. 8(b). Lauritzen Z test [41] is thus employed as follows.

$$Z \approx 10^3 \left(\frac{L}{2a_0}\right)^2 \exp\left(-\frac{X}{T_c\,\Delta T}\right) \tag{12}$$

where L is the effective lamellar width and a_0 is the width of the molecular chain in the crystal. According to this test, regime I crystallization kinetics are followed if the substitution of $X = K_g$ into the test results in $Z \leqq 0.01$. If with $X = 2K_g$ the test contains $Z \geqq 1.0$, regime II kinetics are followed. PA6 as a polycrystalline polymer has α-crystals and γ-crystals, with the former corresponding to $a = 0.956$ nm, $b = 1.724$ nm and $c = 0.801$ nm and the latter corresponding to $a = 0.472$ nm, $c = 1.688$ nm [2,42,43]. As manifested in Fig. 10(a), for non-isothermal crystallization PA6 is mainly represented by α-crystals, so $a = 0.956$ nm and $b = 1.724$ nm are adopted for this study. It can thus be found out that the crystallization of neat PA6 belongs to the crystallizing regime I. Since there are less than 10% of HNTs (a rather small proportion) in PA6/HNTs nanocomposites, the crystallization of PA6/HNTs nanocomposites are also supposed to belong to the crystallizing regime I. The value of $\sigma\sigma_e$ can be obtained by using Eq. (7) and is then listed in Table 4. The product of $\sigma\sigma_e$ can be split by using the empirical relationship [44]:

$$\sigma = 0.11\,\Delta h_f^0 \sqrt{ab}$$

which allows evaluation of lateral surface free energy form the parameters a and b of the PA6 unit cell. The σ was calculated as $3.3 \times 10^{-2}\,\mathrm{J\,m^{-2}}$. The values for σ_e were also summarized in Table 4. It turns out that the values of σ_e of PA6/HNTs nanocomposites are always higher than that of neat PA6. This suggests that there is a strong interaction between HNTs and PA6 molecule segments and that such tendency is weakened at higher HNTs loading.

3.3. Dependence of crystallinity on the cooling rate

The crystallinity of neat PA6 and PA6/HNTs composites can be calculated by means of the following equation based upon DSC data.

$$X_c(\%) = \frac{\Delta H_c}{(1-\phi)\,\Delta H_m} \times 100 \tag{13}$$

where ΔH_c stands for crystallization heat enthalpy, ϕ for the percentage of HNTs, ΔH_m for melting enthalpy of 100% crystallization sample. Since PA6 falls into two types, α-phase crystal and γ-phase crystal, and for this reason, an average melting enthalpy of 190 J/g has been chosen for ΔH_m [45,46]. There several values were proposed for the enthalpy of melting for the different 100% crystalline polymorphic forms of PA6, an intermediate value of 190 J/g was reported by Ioune [45], using several PA6 samples with different molecular weights and crystallinity degrees and plotting the heat of fusion obtained by calorimetric techniques from the area under the peak against the crystallinity determined by density measurements.

Fig. 9 shows the crystallinity of neat PA6 and PA6/HNTs nanocomposites at various cooling rates based on DSC data. As for neat PA6, the higher the cooling rate is, the lower the crystallinity becomes, which is certainly in accordance with usual observances.

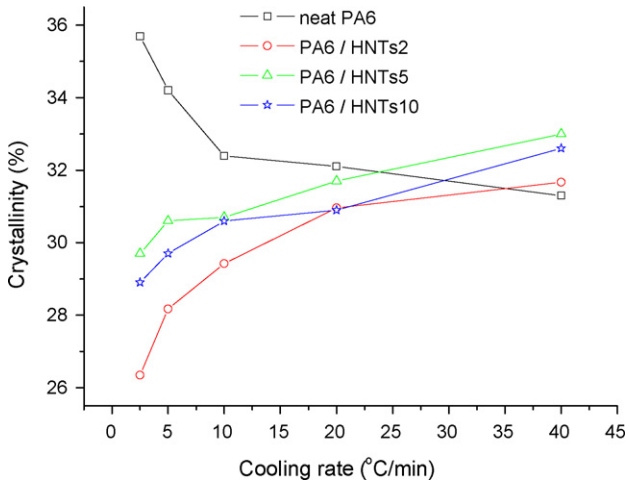

Fig. 9. Crystallinities of neat PA6 and PA6/HNTs nanocomposites at various cooling rates, based on DSC data.

But the crystallinity of the PA6/HNTs nanocomposites increase with the cooling rate. As is evident, HNTs content matter, and the 5 phr of HNTs content affect the crystallinity most. Wu et al. [47,48] have detected and also discussed the same phenomenon for PA6/O-MMT nanocomposites. Paul [21] and Akkapeddi [49] have spotted similar phenomena on the surface of injection samples and in sheet samples of PA6/O-MMT nanocomposites, insisting that sheet-shaped montmorillonite when exposed to high shear stress can cause high orientation of PA6 molecules and thus there is the improved crystallinity of the samples surface. Nonetheless, all the samples in the present work have been through 5 min heat treatment at 250 °C and eliminated thermal history, hence the absence of any impact from stress concentration or shear stress. With all things considered, one can conclude that there must be some other origins for that. To reveal the accurate crystallinity and polymorphism of the nanocomposites during cooling, XRD experiments are conducted and the results are discussed below.

3.4. Dependence of polymorphism on the cooling rate

Fig. 10 demonstrates XRD spectra of neat PA6 and PA6/HNTs nanocomposites at various cooling rate. The α-phase crystals of PA6 exhibit reflection peaks at $2\theta = 19.9°$ and 23.7°, and γ-phase crystals show reflection peak at $2\theta = 21.3°$ [50,51]. The peak at $2\theta = 24.62°$ in Fig. 10(d) is the HNTs' peak. As presented in the figure, γ-phase crystals are almost invisible for neat PA6, which indicates that under this non-isothermal crystallization conditions, the neat PA6 prefers to form α-phase crystals alone. Different from the neat PA6, both α-phase crystals and γ-phase crystals are visible for PA6/HNTs nanocomposites. Moreover, Fig. 10 shows that the intensity of γ-phase crystal peaks grows more obviously when cooling rate or HNTs content increases, implying that increasing cooling rate or HNTs content can facilitate the growth of γ-phase crystals. However, this case is totally different to the case of PA6/CNTs nanocomposites [13], in that one-dimensional CNTs can increase tremendously the initial crystallization temperature of PA6 but cause little hindrance to the movement of PA6 molecules. As a consequence, PA6 nucleates very soon at the high temperature of over 200 °C to form α-phase crystals with higher thermal stability. By comparison, HNTs as one-dimensional rigid nanotubes, have the surface covered with –Si–O and –OH groups, are capable of forming hydrogen bond with amide groups of PA6 chains. For one thing, the interfacial interaction restrains the mobility of PA6 chains and weakens the hydrogen bonding interactions between the PA6 chains, making it difficult to display an orderly arrangement to pro-

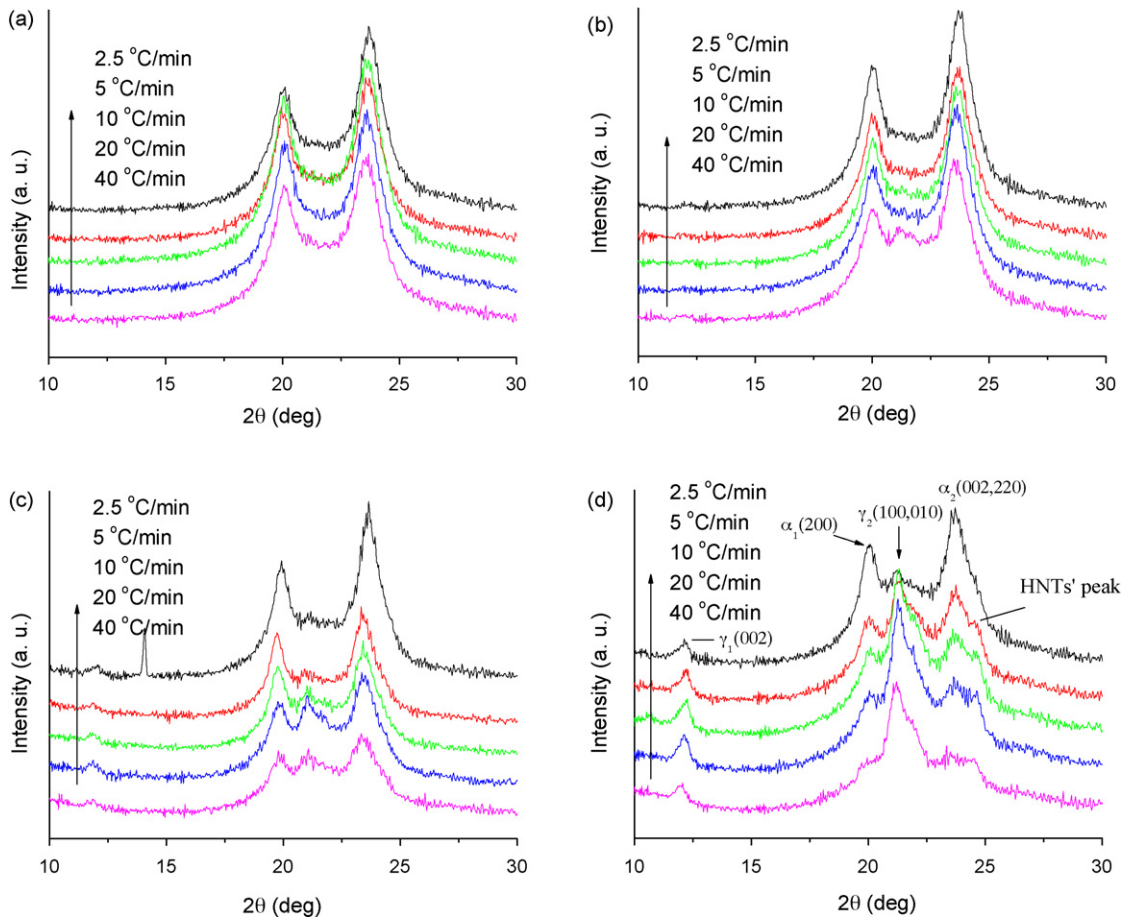

Fig. 10. XRD patterns of PA6 and PA6/HNTs nanocomposites at various cooling rates (a) neat PA6, (b) PA6/HNTs2, (c) PA6/HNTs5 and (d) PA6/HNTs10.

duce α-phase crystals. This may be substantiated by the FTIR result in Fig. 11 As shown, compared with the neat PA6, peak at 3296 cm^{-1} characterizing α-phase (N–H stretching) [52] is decreased in the PA6/HNTs nanocomposites, indicating that the addition of HNTs limits the formation of hydrogen-bonded sheets in PA6 matrix.

Based on XRD data, the crystallinity of neat PA6 and PA6/HNTs nanocomposites is calculated and listed in Table 5 by adopting the following equation, and the proportion of γ-phase crystals in the total crystallinity is listed in Table 6:

$$X_c(\%) = \frac{\sum(A_{\alpha\text{-form}} + A_{\gamma\text{-form}})}{\sum(A_{\alpha\text{-form}} + A_{\gamma\text{-form}} + A_{\text{amorph}})} \times 100 \quad (14)$$

where $A_{\alpha\text{-form}}$, $A_{\gamma\text{-form}}$ and A_{amorph} represent α-phase crystals, γ-phase crystals, and amorphous area, respectively.

Table 5 reveals that, as cooling rate increases, the crystallinity of neat PA6 decreases, while as cooling rate increases, the crystallinity of PA6/HNTs nanocomposites increases, which is in good agreement

Table 5
Crystallinities calculated from XRD spectra of neat PA6 and PA6/HNTs nanocomposites.

Samples	Cooling rate				
	2.5 °C/min	5 °C/min	10 °C/min	20 °C/min	40 °C/min
Neat PA6	47.36	44.50	42.58	40.66	39.76
PA6/HNTs2	41.50	43.76	45.60	49.72	51.81
PA6/HNTs5	47.20	50.25	51.45	55.26	58.67
PA6/HNTs10	39.80	44.90	50.10	55.80	57.22

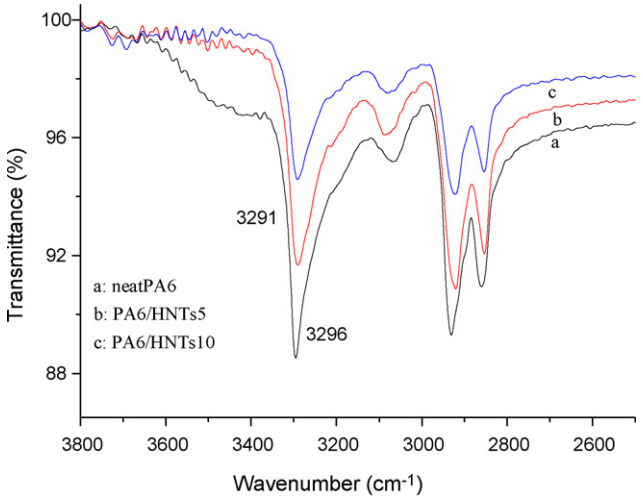

Fig. 11. FTIR spectra of neat PA6 and PA6/HNTs nanocomposites (all samples are injection molded specimen).

Table 6
Values of [γ/(γ+α)]% calculated from XRD spectra of neat PA6 and its nanocomposites.

Samples	Cooling rate				
	2.5 °C/min	5 °C/min	10 °C/min	20 °C/min	40 °C/min
Neat PA6	3.85	5.66	9.91	11.50	15.97
PA6/HNTs2	9.91	14.53	18.03	20.63	23.08
PA6/HNTs5	13.04	15.25	17.36	25.37	29.08
PA6/HNTs10	37.11	44.75	57.63	64.91	65.87

with DSC data as mentioned above. In addition, we realize from Table 6 that the proportion of γ-phase crystals in the total crystallinity grows instantly as cooling rate and HNTs content increases. As a consequence, it is mainly the γ-phase crystals that contribute to the rise of crystallinity of PA6/HNTs nanocomposites. In view of that, it can be concluded that it is because of the multiple roles of HNTs play in non-isothermal crystallization that the crystallinity of PA6/HNTs nanocomposites increases as cooling rate increases. It is believed that there are three main roles of HNTs in affecting the crystallization behavior of the PA6. First, HNTs serve as nucleating agent, resulting higher T_0; second, there is an enthalpic interaction between the PA6 and the HNT, resulting restricted mobility of PA6 chains; Finally and more importantly, HNTs favor the formation of the gamma phase.

4. Conclusion

Non-isothermal crystallization and the polymorphism of the PA6 and the PA6/HNTs nanocomposites are studied by adopting DSC analysis, XRD analysis and POM observations. The kinetic data were computed by the Hoffman–Lauritzen nucleation theory. HNTs not only act as nucleating agents, but also reduce mobility of the PA6 chains due to the strong interaction between HNTs and PA6 chains. HNTs accelerate the crystallization in the concentration range studied. The kinetics analysis indicates that the fold-surface free energy of PA6/HNTs nanocomposites is larger than that of neat PA6. The increasing tendency of the fold-surface free energy of PA6/HNTs nanocomposites is restricted at higher HNTs loading. Interestingly, the crystallinity of the PA6/HNTs nanocomposites increases with cooling rate. HNTs content is found to exert a great effect upon the crystallinity of the PA6/HNTs nanocomposites, and, the more proportion HNTs content takes up, the larger percentage γ-phase crystals may have of total crystals. The crystallization behavior of the PA6/HNTs nanocomposites is correlated with the multiple roles HNTs play in the crystallization.

Acknowledgment

We are grateful for the financial support by the National Natural Science Foundation of China with grant number of 50603005.

References

[1] C.W. Bunn, E.V. Garner, Proc. R. Soc. Lond. A 189 (1947) 39.
[2] H. Arimoto, M. Ishibashi, M. Hirai, Y. Chatani, J. Polym. Sci. Part A 3 (1965) 317.
[3] T. Liu, I.Y. Phang, W.D. Zhang, Macromolecules 37 (2004) 7214.
[4] H. Meng, R. Yang, Polymer 49 (2008) 610.
[5] P.V. Kodgier, A.R. Bhattacharyya, A. Misra, Chem. Phys. Lett. 432 (2006) 480.
[6] A.R. Bhattacharyya, P. Potschke, Macromol. Symp. 233 (2006) 161.
[7] C.G. Zhao, G.J. Hu, D.W. Schaefer, C.C. Han, Polymer 46 (2005) 5125.
[8] G.M. Kim, G.H. Michler, Polymer 48 (2007) 4814.
[9] A.N. Wilkinson, Z. Man, P. Matikainen, Macromol. Mater. Eng. 291 (2006) 917.
[10] H. Fong, W.D. Liu, R.A. Vaia, Polymer 43 (2002) 775.
[11] C. Ibanes, L. David, G. Robert, J. Polym. Sci. Polym. Phys. 42 (2004) 3876.
[12] B.C. Guo, Q.L. Zou, Y.D. Lei, et al., New Chem. Mater. 6 (2008) 32 (in Chinese).
[13] I.Y. Phang, J. Ma, W.D. Zhang, Polym. Int. 55 (2006) 71.
[14] X.F. Lu, J.N. Hay, Polymer 42 (2001) 9423.
[15] M.L. Di Lorenzo, C. Silvestre, Prog. Polym. Sci. 24 (1999) 917.
[16] J. Li, Z.P. Fang, F. Liu, Eur. Polym. J. 42 (2006) 3230.
[17] J. Li, Z.P. Fang, F. Liu, J. Appl. Polym. Sci. 105 (2007) 3531.
[18] D.M. Lincoln, R.A. Vaia, Z.G. Wang, B.S. Hsiao, R. Krishnamoorti, Polymer 42 (2001) 9975.
[19] T.X. Liu, Z.H. Liu, K.X. Ma, L. Shen, K.Y. Zeng, C.B. He, Compos. Sci. Technol. 63 (2003) 331.
[20] T.X. Liu, S.K. Yan, M. Bonnet, I. Lieberwirth, K.D. Rogausch, J. Petermann, J. Mater. Sci. 35 (2000) 5047.
[21] T.D. Fornes, D.R. Paul, Polymer 44 (2003) 3945.
[22] X.H. Liu, Q.J. Wu, Eur. Polym. J. 38 (2002) 1383.
[23] M.X. Liu, B.C. Guo, M.L. Du, X.J. Cai, D.M. Jia, Nanotechnology 18 (2007) 455703.
[24] M.X. Liu, B.C. Guo, Q.L. Zou, M.L. Du, D.M. Jia, Nanotechnology 19 (2008) 205709.
[25] M.L. Du, B.C. Guo, D.M. Jia, Eur. Polym. J. 42 (2006) 1362.
[26] M.L. Du, B.C. Guo, M.X. Liu, D.M. Jia, Polym. Polym. Compos. 15 (2007) 321.
[27] G. Gurato, A. Fichera, F.Z. Grandi, R. Zanetti, P. Canal, Macromol. Chem. 175 (1974) 953.
[28] D.M. Lincoln, R.A. Vaia, R. Krishnamoorti, Macromolecules 37 (2004) 4554.
[29] M. Avrami, J. Chem. Phys. 7 (1939) 1103.
[30] A. Jeziorny, Polymer 19 (10) (1978) 1142.
[31] T. Ozawa, Polymer 12 (1971) 150.
[32] T. Ozawa, Polymer 19 (1978) 1142.
[33] J. Liu, Z. Mo, Acta Polym. Sin. 1 (1993) 1.
[34] J.D. Hoffman, G.T. Davis, J.I. Lauritzen Jr., in: N.B. Hannay (Ed.), Treatise on Solid State Chemistry, vol. 3, Plenum, New York, 1976, p. 497.
[35] S. Vyazovkin, N. Sbirrazzuoli, Macromol. Rapid Commun. 25 (2004) 733.
[36] S. Vyazovkin, D. Dollimore, J. Chem. Inf. Comp. Sci. 36 (1996) 42.
[37] S. Vyazovkin, J. Comput. Chem. 18 (1997) 393.
[38] S. Vyazovkin, J. Comput. Chem. 22 (2001) 178.
[39] C.D. Doyle, J. Appl. Polym. Sci. 6 (1962) 639.
[40] W.G. Weng, G.H. Chen, D.J. Wu, Polymer 44 (2003) 8119.
[41] J.I. Lauritzen, J. Appl. Phys. 44 (1973) 4353.
[42] D.R. Holmes, C.W. Bunn, D.J. Smith, J. Polym. Sci. 17 (1955) 159.
[43] M.I. Kohen (Ed.), Nylon Plastics Handbook, Hanser, New York, 1995.
[44] J.D. Hoffman, G.T. Davis, J.I. Lauritzen, in: H.B. Hannay (Ed.), Treatise on Solid State Chemistry, vol. 3, Plenum Press, New York, 1975 (Chapter 6).
[45] M. Inoue, J. Polym. Sci. Part A 2 (7) (1969) 1755.
[46] I. Campoy, M.A. Gomez, C. Marco, Polymer 39 (1998) 6279.
[47] Q.J. Wu, X.H. Liu, L.A. Berglund, Macromol. Rapid Commun. 22 (2001) 1438.
[48] X.H. Liu, Q.J. Wu, L.A. Berglund, Macromol. Mater. Eng. 287 (2002) 515.
[49] M.K. Akkapeddi, ANTEC 99 Conference, New York, May 1999, p. 1619.
[50] I. Campoy, M.A. Gomez, C. Macro, Polymer 40 (1999) 4259.
[51] I. Campoy, M.A. Gomez, C. Macro, Polymer 39 (1998) 6279.
[52] Q.J. Wu, X.H. Liu, A. Lars, Berglund. Polymer 43 (2002) 2445.